### Science and Technology Indonesia

e-ISSN:2580-4391 p-ISSN:2580-4405 Vol. 10, No. 4, October 2025



Research Paper



# Significant Reduction in Lattice Thermal Conductivity of (PbTe)<sub>0.95</sub> - (PbS)<sub>0.05</sub> Thermoelectric Materials Through Liquid Silicon Quenching

Dianta Ginting<sup>1\*</sup>, Ai Nurlaela<sup>2</sup>, Dwi Nanto<sup>2</sup>, Mashadi<sup>3</sup>, Toto Sudiro<sup>3</sup>, Tony Kristiantoro<sup>4</sup>, Jong-Soo Rhyee<sup>5</sup>

#### **Abstract**

Thermoelectric materials are game-changers, that have the ability to transform waste heat into electrical energy, making them a potential renewable energy solution to reduce reliance on fossil fuels. The standard metric for evaluating thermoelectric materials is the dimensionless figure of merit, ZT, which is markedly influenced by lattice thermal conductivity ( $\kappa_l$ ). Higher thermal transport through the lattice lowers the ZT value, reducing the material's efficiency. Therefore, finding ways to decrease  $\kappa_l$  is critical for boosting thermoelectric performance. In our research, we explored an innovative approach by applying a quenching technique using liquid silicon to reduce thermal conductivity ( $\kappa_T$ ) due to lattice vibrations. We compared the lattice conductivity ( $\kappa_l$ ) of materials with and without this liquid silicon quenching process. The results were striking: at 300 K, quenching lowers the lattice thermal conductivity by about 40.1%, and at 800 K, it is still reduced by roughly 24.7% compared with pristine PbTe. Even more impressive, when compared to non-quenched (PbTe) $_{0.95}$  – (PbS) $_{0.05}$  alloys, at 300 K, the silicon-quenched sample attains an additional  $\kappa_l$  reduction of roughly 16.1%, while at 800 K the extra decrease is about 13.0%. These findings highlight that liquid silicon quenching is a highly effective method for lowering  $\kappa_l$  of PbTe thermoelectric materials. This approach paves the way for developing next-generation thermoelectric materials that are more efficient, particularly for eco-friendly waste heat recovery applications. Our work opens new possibilities for sustainable energy innovation.

#### Keywords

Binary PbTe-PbS System, Lattice Thermal Conductivity, Sustainable Energy, Silicon Quenching, Thermoelectric

Received: 22 April 2025, Accepted: 9 July 2025

https://doi.org/10.26554/sti.2025.10.4.1087-1095

#### 1. INTRODUCTION

The worldwide energy crisis and environmental issues caused by using fossil fuels have accelerated efforts to discover sustainable methods for energy harvesting and conversion (Xiao and Zhao, 2018; Hanus et al., 2019; Parashchuk et al., 2021; Bell, 2008; Snyder and Toberer, 2008). This growing energy crisis and environmental pressures from fossil fuel consumption have intensified global efforts toward sustainable energy alternatives, with fossil fuel availability declining and making the transition to alternative energy sources increasingly urgent (Widianingsih et al., 2024; Jahiding et al., 2024; Telussa et al., 2022). With increasing recognition that energy transition towards renewable and low-carbon fuels is imperative (Rohendi et al., 2024), thermoelectric materials are game-changers, capable of harnessing waste heat to produce electricity. It makes them a potential

renewable energy solution to reduce reliance on fossil fuels. Thermoelectric (TE) materials have become a focal point of research because they provide a solid state means of harvesting waste heat and converting it directly into electricity-without any moving parts-thus offering a practical route to enhance energy efficiency across a wide range of industrial processes (Ginting et al., 2019; Romero et al., 2015; Tan et al., 2016; Zebarjadi et al., 2012).

Thermoelectric performance is typically evaluated using the dimensionless figure of merit, ZT, as shown in Equation (1).

$$ZT = \frac{S^2 \sigma T}{\kappa_T} \tag{1}$$

Here, S represents the Seebeck coefficient,  $\sigma$  denotes elec-

<sup>&</sup>lt;sup>1</sup>Master of Mechanical Engineering Program, Faculty of Engineering, Universitas Mercubuana, West Jakarta, 11650, Indonesia

<sup>&</sup>lt;sup>2</sup>Physics Education Department, Syarif Hidayatullah State Islamic University Jakarta, South Tangerang, 15412, Indonesia

<sup>&</sup>lt;sup>3</sup>Research Center for Advanced Material, National Research and Innovation Agency, South Tangerang, 15310, Indonesia

<sup>&</sup>lt;sup>4</sup>Research Center for Electronics, National Research and Innovation Agency, Bandung, 40135, Indonesia

<sup>&</sup>lt;sup>5</sup>Department of Applied Physics and Institute of Natural Sciences, Kyung Hee University, Yong-in, 17104, South Korea

<sup>\*</sup>Corresponding author: dianta.ginting@mercubuana.ac.id

trical conductivity, T stands for temperature, and  $\kappa_T$  (total thermal conductivity) indicates the combined thermal conductivity, which includes both electronic ( $\kappa_e$ ) and lattice ( $\kappa_l$ ) components. (Ginting et al., 2016; Petsagkourakis et al., 2018; Zhu et al., 2017; Mao et al., 2020).

Thermoelectric devices operating on the principle of thermopower, generating a voltage differential in response to a temperature gradient. The efficiency of these devices is fundamentally limited by the interdependence of transport parameters. It is challenging to simultaneously optimize electrical conductivity and Seebeck coefficient while minimizing thermal conductivity (Pei et al., 2012; Gayner and Kar, 2016; Zhang and Zhao, 2015). Among various strategies to enhance ZT, reducing ( $\kappa_l$ ) has proven particularly effective. It can be independently modified without significantly compromising electron transport properties (Zhang and Zhao, 2015; Li et al., 2020; Zhao et al., 2016). This is especially important because ( $\kappa_l$ ) is typically the primary contributor to thermal conductivity in semiconducting thermoelectric materials (He and Tritt, 2017; Yang et al., 2022).

PbTe has become a preferred thermoelectric material for applications in the 500–850 K range due to its favorable electronic band structure for charge transport and its inherently low total thermal conductivity ( $\kappa_T$ ) (Pei et al., 2011; Biswas et al., 2012; Dughaish, 2002; Heremans et al., 2008). As reported by Chen Chen et al. (2018) and further supported by Delaire et al. (2011), the cubic rock-salt structure of PbTe, combined with its heavy constituent elements and strong anharmonicity, contributes to its relatively low lattice thermal conductivity ( $\kappa_l$ ) of approximately 2.2 W/mK at room temperature. Researchers have explored various strategies to further reduce  $\kappa_l$  in PbTe, including alloying, nanostructuring, and forming composite systems with other materials.

Among these various approaches, the binary PbTe-PbS system has demonstrated exceptional potential. The excellence of this system is primarily attributed to the combined effects of alloying-induced scattering and nanoscale structuring that emerge from phase separation processes. This phenomenon has been verified through a series of comprehensive studies conducted by various research groups (Lee et al., 2013; Johnsen et al., 2011; Ginting et al., 2016, 2019; Samanta et al., 2018; Girard et al., 2021).

The PbTe–PbS binary system demonstrates exceptionally low total thermal conductivity ( $\kappa_T$ ), driven by the synergistic effects of alloying and nanoscale structuring (Lee et al., 2013; Wu et al., 2015). The limited solubility of PbS within PbTe induces the formation of nanoscale precipitates during carefully controlled cooling processes. These precipitates introduce additional interfaces that effectively scatter phonons while preserving the electronic transport properties of the matrix (Johnsen et al., 2011; Yamini et al., 2014). Building on this, Ginting and colleagues investigated quaternary PbTe–PbSe–PbS systems and found that incorporating a small PbS fraction ( $\leq 0.07$ ) leads to the formation of nanoprecipitates within the matrix. This microstructural modification significantly reduces

lattice-based thermal conductivity ( $\kappa_l$ ) without compromising the desirable electronic characteristics of the material (Ginting et al., 2016, 2019; Wang et al., 2019).

Ouenching techniques have become an extremely effective method for tailoring the microstructure and thermal properties of thermoelectric materials (Zhao et al., 2014a; Wu et al., 2014; Tian et al., 2012; Nielsen et al., 2013). By rapidly cooling the material, quenching locks in high-temperature phase arrangements. In addition, it prevents the formation of equilibrium segregations and producing metastable microstructures that enhance phonon scattering. Research has shown that defects and strain fields introduced during quenching can significantly lower  $\kappa_l$  by increasing phonon scattering while largely preserving the material's electrical transport properties (Wu et al., 2014; Korrapati et al., 2022). This strategy has proven successful across various thermoelectric systems, particularly in PbTe-based materials. PbTe-based materials were effective where quenching has led to enhanced thermoelectric performance through carefully optimized microstructural characteristics (Zhao et al., 2014b, 2021; Yang et al., 2020).

In our research, we investigate the effect of quenching using liquid silicon on the lattice thermal conductivity ( $\kappa_l$ ) and thermoelectric properties of (PbTe)<sub>0.95</sub> – (PbS)<sub>0.05</sub> compounds. Liquid silicon, with its distinct atomic size and electronic characteristics compared to the host material, is expected to induce significant local strain fields and point defects when introduced through rapid quenching. This rapid quenching process potentially enhances phonon scattering without adversely affecting electronic transport (Fu et al., 2021; Liu et al., 2022). Our findings demonstrate that this approach offers a promising route to more effectively optimize the thermoelectric performance of PbTe-based materials through strategic microstructural engineering. The results reveal that quenching with liquid silicon significantly reduces lattice thermal conductivity in the composite material-by 40.07 % at room temperature (300 K) and 24.72 % at high temperature (800 K), compared to pristine PbTe. Furthermore, when compared to non-quenched  $(PbTe)_{0.95} - (PbS)_{0.05}$ , the liquid silicon-quenched samples exhibit additional reductions of 16.13% at 300 K and 12.99% at 800 K. This phenomenon highlights the effectiveness of liquid silicon quenching in enhancing phonon scattering across the operational temperature range of these thermoelectric materials.

#### 2. EXPERIMENTAL SECTION

#### 2.1 Materials

Lead, sulfur, tellurium, and sodium with  $5\,\mathrm{N}$  (99.999%) purity, each procured from Sigma-Aldrich, were used as starting reagents for the synthesis.

#### 2.2 Methods

The synthesis of  $(PbTe)_{0.95} - (PbS)_{0.05}$  compounds was conducted using a systematic three-step methodology designed to prevent volatile element loss and achieve compositional uniformity. This approach encompasses precursor preparation, con-

© 2025 The Authors. Page 1088 of 1095

trolled alloy formation, and consolidation through hot-press sintering:

#### 2.2.1 Step 1 – Preparation of PbS Precursors

Ultra-pure lead (Pb) and sulfur (S) (Sigma-Aldrich, 99.999% purity) were portioned in a 1:1 stoichiometric ratio to synthesize PbS. The elemental mixture was sealed in evacuated quartz ampoules (<10<sup>-4</sup> torr), then heated to 1150°C for 10 hours to ensure complete reaction (Ginting et al., 2016, 2019). This vacuum environment prevents oxidation and minimizes sulfur volatilization, yielding homogeneous PbS ingots after furnace cooling.

#### 2.2.2 Step 2 – Synthesis of Target Compositions

Pre-synthesized PbS was mixed with elemental Pb (99.999%), Te (99.999%), and Na (99.999%). All supplied by Sigma-Aldrich at ultra-high purity grades is to form Na-doped compositions with actual stoichiometry of  $Pb_{0.93}Na_{0.02}Te_{0.95}S_{0.05}$ , referred to as  $(PbTe)_{0.95} - (PbS)_{0.05}$  for simplicity. Sodium incorporation at Pb sites generates acceptor states that enhance hole concentration while maintaining structural stability (Yamini et al., 2014; Ginting et al., 2019). The powder mixture was vacuum-sealed (<  $10^{-4}$  torr) and melted at  $1100^{\circ}$ C for 10 hours to ensure complete homogenization.

#### 2.2.3 Step 3 – Quenching and Consolidation

Following synthesis, samples underwent distinct cooling protocols. One group of (PbTe)<sub>0.95</sub> – (PbS)<sub>0.05</sub> samples was rapidly cooled by quenching in liquid silicon. Whereas the control samples, consisting of pristine PbTe and a separate group of (PbTe)<sub>0.95</sub> – (PbS)<sub>0.05</sub>, were allowed to cool slowly to ambient temperature without any quenching. Following quenching, the specimens underwent a 72-hour annealing treatment at 500°C to alleviate thermal stress and attain microstructural equilibrium (Ginting et al., 2019, 2016). All ingots were manually ground to fine powders and consolidated via pressure-assisted sintering using graphite dies (diameter: 12.7 mm) at 500°C under 40 MPa uniaxial load for 1 hour in vacuum atmosphere (Ginting et al., 2019).

#### 2.3 Sample Analysis

For phase and structural analysis, powder X-ray diffraction (XRD) patterns were collected using a D8 Advance instrument from Bruker (AXS GmbH, Karlsruhe, Germany). Measurements were performed with Cu K $\alpha$  radiation ( $\lambda$  = 1.5406 Å), with the X-ray tube operated at 40 kV and 40 mA. For detailed nanoscale morphological analysis, high-resolution transmission electron microscopy (HRTEM) was carried out using a JEOL 2100F field-emission microscope (JEOL Ltd., Tokyo, Japan), operated at an acceleration voltage of 200 kV with a point resolution of 0.19 nm. Sample preparation involved precision ion milling using a Nova 600 NanoLab focused ion beam (FIB) system (FEI Company, Hillsboro, OR, USA) with a Ga<sup>+</sup> ion source, operating at acceleration voltages ranging from 5 to 30 kV to achieve optimal surface quality for imaging. The total thermal conductivity ( $\kappa_T$ ) was calculated using Equation (2):

$$\kappa_T = \rho \lambda C_p \tag{2}$$

where these parameters correspond to the sample's density  $(\rho)$ , thermal diffusivity  $(\lambda)$ , and specific heat capacity  $(C_p)$ , respectively. The density of each specimen was determined using the Archimedes principle via liquid displacement methodology. Thermal diffusivity measurements were conducted using a laser flash apparatus (model LFA-447, NETZSCH, Germany) under controlled temperature conditions. Specific heat capacity was estimated using the classical Dulong–Petit approximation, which provides reliable values for solid crystalline materials within the temperature range investigated.

#### 3. RESULTS AND DISCUSSION

#### 3.1 Phase Identification and Structural Characterization

Figure 1 presents the XRD patterns of pristine PbTe, along with the alloy of composition  $(PbTe)_{0.95} - (PbS)_{0.05}$  in both non-quenched and Si-quenched states. The diffraction data indicate that all specimens retain the characteristic face-centered cubic (FCC) rock-salt structure (NaCl-type) typical of lead chalcogenides, with prominent reflections indexed to the (111), (200), (220), (311), (222), (400), (402), and (422) crystallographic planes. The (200) reflection at approximately 27.5° appears as the dominant peak in all samples, confirming the preservation of the fundamental PbTe crystal structure despite compositional modification and variations in the cooling protocol.

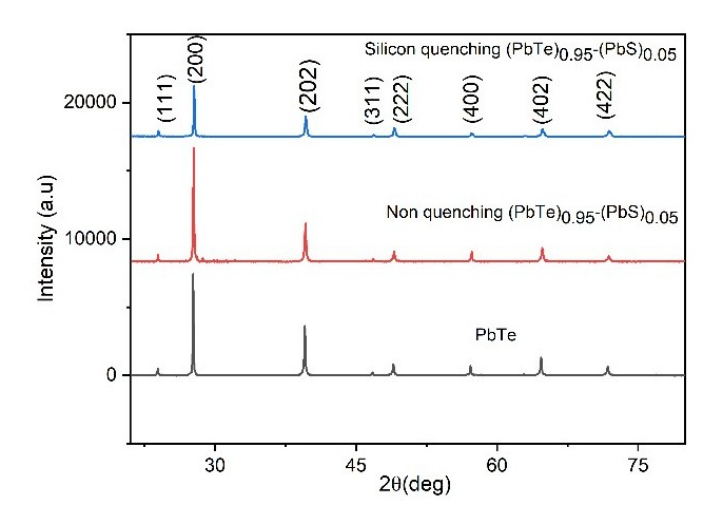


**Figure 1.** X-ray Diffraction (XRD) Profiles for Pristine PbTe, Non-Quenched (PbTe)<sub>0.95</sub> – (PbS)<sub>0.05</sub>, and Silicon-Quenched (PbTe)<sub>0.95</sub> – (PbS)<sub>0.05</sub> Samples

Detailed examination of the diffraction patterns highlights several notable distinctions between samples. The pristine PbTe exhibits particularly sharp diffraction peaks, indicating excellent crystallinity with minimal lattice defects or strain. When comparing the non-quenched  $(PbTe)_{0.95}$  –  $(PbS)_{0.05}$ 

© 2025 The Authors. Page 1089 of 1095

composite to pristine PbTe, we observe slight peak position shifts attributable to lattice parameter adjustments resulting from partial substitution of  $Te^{2^-}$  ions (ionic radius 2.21 Å) with smaller  $S^{2^-}$  ions (ionic radius 1.84 Å). This substitutional effect generates modest lattice contraction while maintaining the parent rock-salt structure, confirming successful formation of a PbTe-PbS solid solution.

The silicon-quenched (PbTe)<sub>0.95</sub> – (PbS)<sub>0.05</sub> sample displays distinctive features compared to its conventionally cooled counterpart. Most significantly, its diffraction peaks exhibit moderate broadening, particularly evident in the (200), (220), and (400) reflections. This broadening phenomenon stems predominantly from two mechanisms. First, the rapid cooling during liquid silicon quenching introduces substantial microstrain into the crystal lattice through the formation of point defects, dislocations, and other structural imperfections. Second, the accelerated cooling inherently restricts grain growth, potentially yielding reduced crystallite dimensions compared to slowly cooled specimens (Biswas et al., 2012; Zhao et al., 2014b). The combined effect creates enhanced phonon scattering centers within the material matrix while preserving the fundamental crystal structure.

## 3.2 TEM Characterization of Silicon-Quenched (PbTe)<sub>0.95</sub>-(PbS)<sub>0.05</sub>

Figure 2 presents the TEM characterization of silicon-quenched  $(PbTe)_{0.95} - (PbS)_{0.05}$ . Low magnified TEM image TEM image (Figure 2a) reveals crystalline regions with visible lattice fringes alongside areas of varying contrast. This indicates strain fields and structural defects induced by rapid silicon quenching. These nanoscale features include localized lattice distortions and potential nanoprecipitates at interfaces, which serve as effective phonon scattering centers.

The corresponding Fast Fourier Transform pattern (Figure 2b) confirms the material's predominantly single-crystalline nature with a face-centered cubic structure, consistent with the XRD-identified rock-salt phase. However, subtle spot elongation and diffuse scattering between primary diffraction points indicate the presence of lattice strain and potential short-range ordering introduced during the quenching process. The TEM analysis reveals that silicon quenching induces a hierarchical range of structural modifications—from atomic-scale defects to nanoscale interfaces—while preserving the fundamental crystal structure. These multiscale features collectively enhance phonon scattering across a broad spectrum of vibrational frequencies. This mechanism accounts for the significant reduction in  $\kappa_l$  observed in the silicon-quenched samples compared to both pristine PbTe and conventionally cooled composites.

### 3.3 Thermal Conductivity ( $\kappa_T$ ) as a Function of Temperature

Figure 3 presents the dependence of total thermal conductivity  $(\kappa_T)$  on temperature for the three investigated samples: pristine PbTe, as well as the non-quenched and Si-quenched states of the  $(PbTe)_{0.95}(PbS)_{0.05}$  alloy. All samples exhibit a decreasing

trend in  $\kappa_T$  with increasing temperature, which is consistent with enhanced phonon–phonon Umklapp scattering processes typical of crystalline semiconductors (Tian et al., 2012).

Figure 3 demonstrates that, over the 300–800 K range, pristine PbTe exhibits greater  $\kappa_T$  than its (PbTe)<sub>0.95</sub>-(PbS)<sub>0.05</sub> counterpart in both untreated and liquid silicon quenched states. At 300 K, pristine PbTe exhibits  $\kappa_T$  of roughly 4.3 Wm<sup>-1</sup>K<sup>-1</sup>, which declines to about 1.3 Wm<sup>-1</sup>K<sup>-1</sup> at 800 K, consistent with established literature values for single-phase lead telluride (Pei et al., 2011). At 300 K, the non-quenched (PbTe) $_{0.95}$ -(PbS)<sub>0.05</sub> composite shows a total thermal conductivity of roughly 3.5 Wm<sup>-1</sup>K<sup>-1</sup>, which decreases to about 1.2 Wm<sup>-1</sup>K<sup>-1</sup> at 800 K. Liquid silicon quenching of the (PbTe)<sub>0.95</sub>(PbS)<sub>0.05</sub> alloy yields the largest drop in overall  $\kappa_T$ , reaching 3.1 Wm<sup>-1</sup>K<sup>-1</sup> at 300 K and declining further to 1.1 Wm<sup>-1</sup>K<sup>-1</sup> at 800 K. This represents reductions of 40.07% at 300 K and 24.72% at 800 K compared to pristine PbTe, as well as further reductions of 16.13% at 300 K and 12.99% at 800 K relative to the nonquenched composite. The decrease in  $\kappa_T$  is ascribed to multiple phonon-scattering processes, including enhanced point defect scattering, strain fields, and potential nanoprecipitates formed during rapid cooling (Biswas et al., 2012; Zhao et al., 2014a).

To better understand the significance of our  $\kappa_T$  reduction, Table 1 presents a comprehensive comparison of  $\kappa_T$  values for our materials alongside other representative chalcogenide thermoelectric materials. The comparison reveals the progressive improvement achieved through our processing approach, starting from pristine PbTe (4.28 Wm<sup>-1</sup>K<sup>-1</sup> at 300 K), followed by the non-quenched composite (3.50 Wm<sup>-1</sup>K<sup>-1</sup>), and finally our silicon-quenched material (3.12 Wm<sup>-1</sup>K). When positioned within the broader chalcogenide family, our material demonstrates competitive performance while maintaining superior temperature stability. While Se-based SnSe exhibits the lowest  $\kappa_T$  (0.70 Wm<sup>-1</sup>K<sup>-1</sup> at 300 K), and S-based SnS shows values of 1.36 Wm<sup>-1</sup>K<sup>-1</sup>, our PbTe-based system offers advantages in terms of processing scalability and mid-temperature operational stability. Notably, our material demonstrates superior temperature behavior compared to Te-based Bi<sub>2</sub>Te<sub>3</sub>, which shows an unfavorable increase from 1.58 to 2.76 Wm<sup>-1</sup>K<sup>-1</sup> with increasing temperature. This comparison validates the effectiveness of our silicon quenching approach in optimizing thermal transport properties within the PbTe system while positioning our material competitively within the chalcogenide thermoelectric materials landscape.

As the temperature approaches 800 K,  $\kappa_T$  values for all compositions converge, indicating that lattice Umklapp scattering becomes the dominant heat transfer mechanism in this high-temperature regime. This effect increasingly overshadows the influence of microstructural changes resulting from compositional adjustments and quenching processes. Nevertheless, the silicon-quenched sample maintains the lowest  $\kappa_T$  throughout the entire temperature range relevant for mid-temperature thermoelectric applications, highlighting the effectiveness of liquid silicon quenching as a processing strategy for reducing

© 2025 The Authors. Page 1090 of 1095

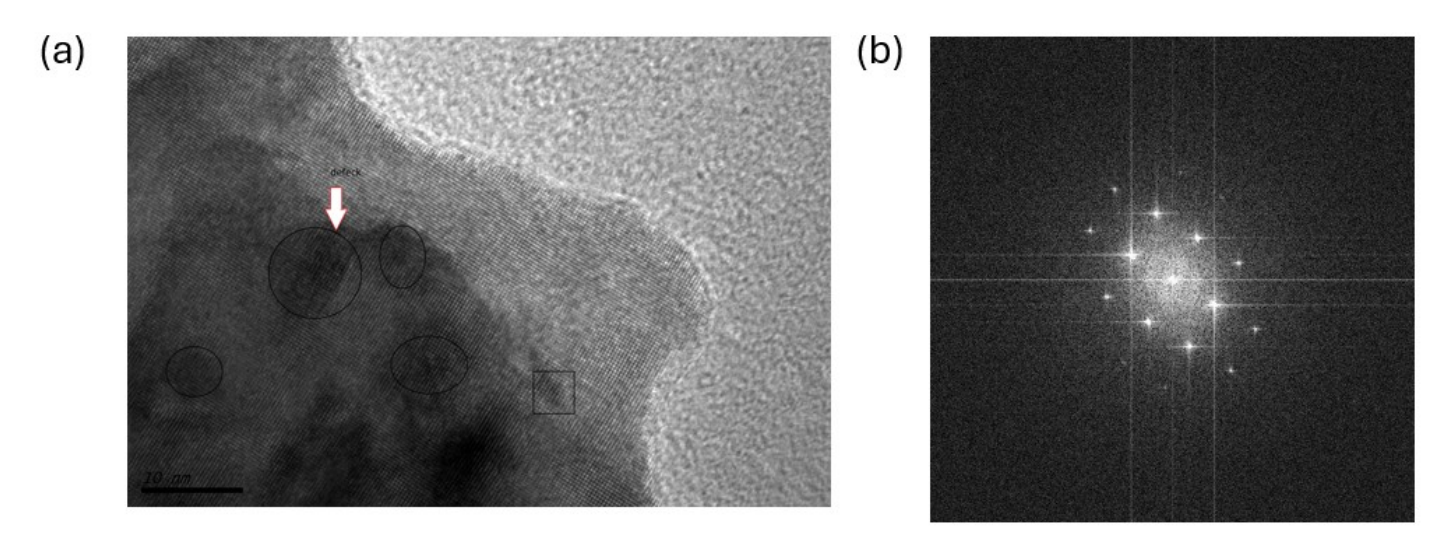


Figure 2. Transmission Electron Microscopy Analysis of Silicon-Quenched (PbTe) $_{0.95}$  – (PbS) $_{0.05}$ : (a) Low Magnified TEM Image (b) Corresponding Fast Fourier Transform (FFT)

**Table 1.** Comparative Analysis of Overall ( $\kappa_T$ ) among Various Chalcogenide Thermoelectric Materials.

Chalcogenide Type	Material System	$\kappa_T \; (\mathrm{Wm^{-1} \; K^{-1}}) \; \mathrm{at}$ 300 K	$\kappa_T$ (Wm <sup>-1</sup> K <sup>-1</sup> ) at High Temperature	Ref
Pb-based	PbTe	4.28	1.32	This Work
Pb-based	(PbTe) <sub>0.95</sub> - (PbS) <sub>0.05</sub> (non-quenched)	3.50	1.27	This Work
Pb-based	(PbTe) <sub>0.95</sub> – (PbS) <sub>0.05</sub> (Si-quenched)	3.12	1.18	This Work
S-based Chalcogenides	SnS	1.36	0.86 (754 K)	(Sasidharan et al., 2025)
Se-based Chalcogenides	SnSe (b-axis)	0.70	0.34 (937 K)	(Zhao et al., 2014a)
Te-based Chalcogenides	$\mathrm{Bi}_{2}\mathrm{Te}_{3}$	1.58	2.76 (520 K)	(Han et al., 2017)

 $\kappa_T$  in PbTe (Ginting et al., 2019).

The  $\kappa_T$  comprises both the lattice (phonon) and electronic contributions. To isolate  $\kappa_l$ , we calculated the electronic thermal conductivity ( $\kappa_e$ ) using the Wiedemann–Franz relationship, expressed as  $\kappa_e = L\sigma T$ , where  $\sigma$  represents electrical conductivity, T is the absolute temperature, and L is the Lorenz number. Under the assumption of a parabolic band structure with acoustic phonon scattering, the Lorenz number was determined using established methods outlined in prior studies (Kim et al., 2014; Lee et al., 2015), as shown in Equation (3).

$$L = \left(\frac{k_B}{e}\right)^2 \left[ \frac{\left(r + \frac{7}{2}\right) F_{r+5/2}(\eta)}{\left(r + \frac{3}{2}\right) F_{r+1/2}(\eta)} - \left(\frac{\left(r + \frac{5}{2}\right) F_{r+3/2}(\eta)}{\left(r + \frac{3}{2}\right) F_{r+1/2}(\eta)}\right)^2 \right]$$
(3)

The scattering parameter (r) governs the nature of carrier scattering, while the reduced Fermi energy,  $\eta = \frac{E_F}{k_B T}$ , repre-

sents the Fermi energy  $(E_F)$  normalized by the product of the Boltzmann constant  $(k_B)$  and absolute temperature (T). The n-order Fermi integral, denoted as  $F_n(\eta)$ , is defined by the standard expression used in semiconductor physics to describe carrier statistics, given in Equation (4) (Kim et al., 2014; Lee et al., 2015):

$$F_n(\eta) = \int_0^\infty \frac{x^n}{1 + e^{x - \eta}} \, dx \tag{4}$$

For acoustic phonon scattering, the carrier scattering exponent is fixed at  $r = -\frac{1}{2}$ . The reduced Fermi level  $(\eta)$  is then extracted by fitting the measured Seebeck coefficient to the transport model outlined by Kim et al. (2014) and Lee et al. (2015), as summarized in Equation (5).

© 2025 The Authors. Page 1091 of 1095

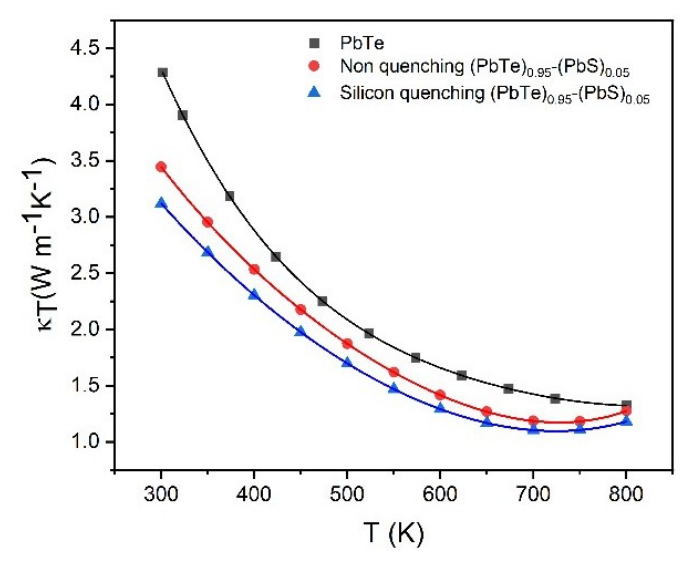


**Figure 3.** Total Thermal Conductivity  $((\kappa_T))$  as a Function of Temperature for Pristine PbTe, Non-Quenched  $(PbTe)_{0.95} - (PbS)_{0.05}$ , and Silicon-Quenched  $(PbTe)_{0.95} - (PbS)_{0.05}$  Over the Temperature Range of 300 K to 800 K

$$S = \pm \frac{k_B}{e} \left\{ \frac{(r + \frac{5}{2}) F_{r + \frac{3}{2}}(\eta)}{(r + \frac{3}{2}) F_{r + \frac{1}{2}}(\eta)} - \eta \right\}$$
 (5)

Figure 4 presents the dependence of  $\kappa_l$  on temperature for pristine PbTe, non-quenched and silicon-quenched (PbTe)<sub>0.95</sub> (PbS)<sub>0.05</sub>, which were obtained by subtracting the electronic contribution from  $\kappa_T$  using the calculated Lorenz numbers. The lattice thermal conductivity exhibits a significant reduction across samples and decreases with increasing temperature for all materials, following the expected  $T^{-1}$  relationship typical of phonon-phonon Umklapp scattering in crystalline solids.

For the undoped (pristine) PbTe sample-the one with the greatest  $\kappa_l$ -it is roughly 2.8 Wm<sup>-1</sup>K<sup>-1</sup> at 300 K and gradually declines to about 0.9 Wm<sup>-1</sup>K<sup>-1</sup> by 800 K. At 300 K, the non-quenched composite containing 5 mol% PbS exhibits a lattice thermal conductivity of roughly 2.0 Wm<sup>-1</sup>K<sup>-1</sup>, whereas at 800 K the value declines to about 0.75 Wm<sup>-1</sup>K<sup>-1</sup>. At 300 K, the reduction is about 28.6%, whereas at 800 K it is roughly 16.7% relative to pristine PbTe, primarily attributed to point defect scattering arising from mass and size differences between S and Te atoms in the crystal lattice.

Figure 4 illustrates that the silicon-quenched (PbTe)<sub>0.95</sub> – (PbS)<sub>0.05</sub> exhibits the lowest lattice thermal conductivity,  $\kappa_l$ , compared to both pristine PbTe and the non-quenched (PbTe)<sub>0.95</sub> – (PbS)<sub>0.05</sub>. Specifically, at 300 K, its  $\kappa_l$  is roughly 1.7 Wm<sup>-1</sup> $K^{-1}$ , dropping to about 0.65 Wm<sup>-1</sup> $K^{-1}$  at 800 K. This corresponds to a 39.3% decrease at 300 K, whereas at 800 K the reduction is roughly 27.8% compared to pristine

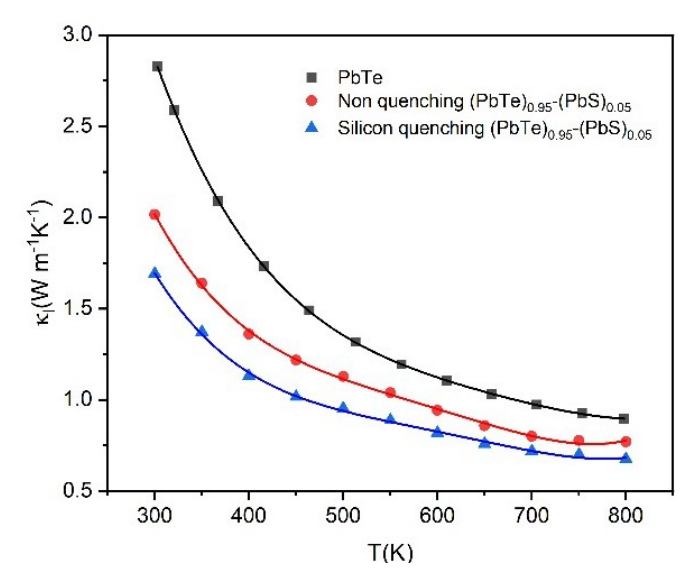


**Figure 4.** Variation of Lattice Thermal Conductivity (( $\kappa_L$ )) with Temperature for Pristine PbTe, Non-Quenched (PbTe)<sub>0.95</sub> – (PbS)<sub>0.05</sub>, and Silicon-Quenched (PbTe)<sub>0.95</sub> – (PbS)<sub>0.05</sub> Alloys

PbTe. More importantly, when compared to the non-quenched  $(PbTe)_{0.95} - (PbS)_{0.05}$  composite, the silicon-quenched sample shows further reductions of 15.0% at 300 K and 13.3% at 800 K. This demonstrates the additional phonon scattering mechanisms introduced by the silicon quenching process.

The enhanced phonon scattering in the silicon-quenched sample can be attributed to several mechanisms observed in microstructural analysis. First, the rapid cooling during silicon quenching generates a higher concentration of point defects. It includes vacancies and interstitial defects, which effectively scatter high-frequency phonons. Second, the strain fields and lattice distortions evident in the TEM analysis create localized variations in atomic spacing that scatter mid-frequency phonons. Finally, potential nanoprecipitates and interfaces formed during the quenching process provide barriers for long-wavelength, low-frequency phonons.

It is important that the relative difference in  $\kappa_l$  between the samples persists across the entire temperature range, although it slightly diminishes at higher temperatures. This observation suggests that intrinsic phonon-phonon Umklapp scattering becomes increasingly dominant at elevated temperatures. Meanwhile, the additional scattering mechanisms introduced by composition modification and quenching continue to play a significant role in reducing phonon transport throughout the temperature range relevant for thermoelectric applications.

The exceptionally low  $\kappa_l$  achieved in the silicon-quenched (PbTe)<sub>0.95</sub> – (PbS)<sub>0.05</sub> samples, particularly at operating temperatures for thermoelectric devices (500-800 K), highlights the effectiveness of liquid silicon quenching as a processing strategy for optimizing the thermal transport properties of PbTe-based thermoelectric materials.

© 2025 The Authors. Page 1092 of 1095

#### 4. CONCLUSIONS

In this study, we examine how silicon quenching treatment modifies the lattice thermal conductivity ( $\kappa_l$ ) of the (PbTe)<sub>0.95</sub>-(PbS)<sub>0.05</sub> solid solution. A comprehensive analysis of the structural, microstructural, and thermal transport properties has vielded several significant findings with important implications for thermoelectric materials development. Our thermal transport measurements and analysis demonstrated that silicon quenching substantially reduces  $\kappa_l$  of (PbTe)<sub>0.95</sub> – (PbS)<sub>0.05</sub>. The silicon-quenched (PbTe) $_{0.95}$  – (PbS) $_{0.05}$  samples demonstrated significantly lower  $\kappa_l$ , with values of 1.7 Wm<sup>-1</sup>K<sup>-1</sup> at room temperature (300 K) and 0.65 Wm<sup>-1</sup>K<sup>-1</sup> at high temperature (800 K). These figures reflect notable reductions of 40.07% at 300 K and 24.47% at 800 K compared to pristine PbTe. Additionally, reductions of 16.13% at 300 K and 12.99% at 800 K were observed relative to the non-quenched  $(PbTe)_{0.95} - (PbS)_{0.05}$  composite. This substantial decrease in  $\kappa_l$  results from a combination of phonon scattering mechanisms caused by the silicon quenching process. These include increased point defect scattering, strain field effects, and scattering at interfaces. The findings highlight silicon quenching as a highly effective method for lowering  $\kappa_l$  in PbTe-based thermoelectric materials while maintaining their electronic transport properties. This technique provides a valuable approach for enhancing the thermoelectric figure of merit (ZT) by selectively optimizing thermal transport without adversely affecting electrical properties.

#### 5. ACKNOWLEDGMENT

We sincerely acknowledge the support of all colleagues and institutions that contributed to the completion of this work. In particular, we extend our gratitude to Universitas Mercu Buana for providing the necessary research infrastructure and administrative support.

#### REFERENCES

- Bell, L. E. (2008). Cooling, Heating, Generating Power, and Recovering Waste Heat with Thermoelectric Systems. Science, 321(5895); 1457–1461
- Biswas, K., J. He, I. D. Blum, C.-I. Wu, T. P. Hogan, D. N. Seidman, V. P. Dravid, and M. G. Kanatzidis (2012). High-Performance Bulk Thermoelectrics with All-Scale Hierarchical Architectures. *Nature*, 489(7416); 414–418
- Chen, Z., X. Zhang, and Y. Pei (2018). Manipulation of Phonon Transport in Thermoelectrics. *Advanced Materials*, **30**(43); 1705617
- Delaire, O., J. Ma, K. Marty, A. F. May, M. A. McGuire, M.-H. Du, D. J. Singh, A. Podlesnyak, G. Ehlers, M. D. Lumsden, and B. C. Sales (2011). Giant Anharmonic Phonon Scattering in PbTe. *Nature Materials*, **10**(8); 614–619
- Dughaish, Z. H. (2002). Lead Telluride as a Thermoelectric Material for Thermoelectric Power Generation. *Physica B: Condensed Matter*, **322**(1–2); 205–223

- Fu, C., H. Wu, Y. Liu, J. He, X. Zhao, and T. Zhu (2021). Enhancing Thermoelectric Properties by Engineering Crystal Defects. *Advanced Science*, 8(1); 2002328
- Gayner, C. and K. K. Kar (2016). Recent Advances in Thermoelectric Materials. *Progress in Materials Science*, **83**; 330–382
- Ginting, D., C.-C. Lin, L. Rathnam, B.-K. Yu, S.-J. Kim, R. A. Al Orabi, and J.-S. Rhyee (2016). Enhancement of Thermoelectric Properties by Effective K-Doping and Nano Precipitation in Quaternary Compounds of (Pb<sub>1-x</sub>K<sub>x</sub>Te)<sub>0.70</sub>(PbSe)<sub>0.25</sub>(PbS)<sub>0.05</sub>. RSC Advances, **6**(67); 62958–62967
- Ginting, D., C.-C. Lin, and J.-S. Rhyee (2019). Synergetic Approach for Superior Thermoelectric Performance in PbTe-PbSe-PbS Quaternary Alloys and Composites. *Energies*, **13**(1); 72
- Girard, S. N., K. Schmidt-Rohr, T. C. Chasapis, E. Hatzikraniotis, B. Njegic, E. M. Levin, A. Rawal, K. M. Paraskevopoulos, and M. G. Kanatzidis (2021). Analysis of Phase Separation in High-Performance PbTe-PbS Thermoelectric Materials. Advanced Functional Materials, 31(13); 2100258
- Han, M.-K., Y. Jin, D.-H. Lee, and S.-J. Kim (2017). Thermoelectric Properties of Bi<sub>2</sub>Te<sub>3</sub>: CuI and the Effect of Its Doping with Pb Atoms. *Materials*, **10**(11); 1235
- Hanus, R., M. T. Agne, A. J. E. Rettie, and et al. (2019). Lattice Softening Significantly Reduces Thermal Conductivity and Leads to High Thermoelectric Efficiency. *Advanced Materials*, 31(21): 1900108
- He, J. and T. M. Tritt (2017). Advances in Thermoelectric Materials Research: Looking Back and Moving Forward. Science, 357(6358); eaak9997
- Heremans, J. P., V. Jovovic, E. S. Toberer, A. Saramat, K. Kurosaki, A. Charoenphakdee, S. Yamanaka, and G. J. Snyder (2008). Enhancement of Thermoelectric Efficiency in PbTe by Distortion of the Electronic Density of States. *Science*, 321(5888); 554–557
- Jahiding, M., M. Mashuni, H. Hamid, W. O. S. Ilmawati, and R. Hamdana (2024). The Production of Renewable Fuels Sago Dregs and Low-Density Polyethylene by Pyrolysis and Its Characterization. *Science and Technology Indonesia*, 9(3); 565–576
- Johnsen, S., J. He, J. Androulakis, V. P. Dravid, I. Todorov, D. Y. Chung, and M. G. Kanatzidis (2011). Nanostructures Boost the Thermoelectric Performance of PbS. *Journal of the American Chemical Society*, 133(10); 3460–3470
- Kim, J. H., M. J. Kim, S. Oh, and J.-S. Rhyee (2014). Thermoelectric Properties of Se-Deficient and Pb-/Sn-Codoped In<sub>4</sub>Pb<sub>0.01</sub>Sn<sub>0.03</sub>Se<sub>3-x</sub> Polycrystalline Compounds. *Journal of Alloys and Compounds*, **615**; 933–936
- Korrapati, V., G. Sumanasekera, and M. K. Sunkara (2022). Recent Advances in Bulk Thermoelectric Materials: Strategies to Enhance Figure of Merit. *Dalton Transactions*, **51**(8); 2845–2869
- Lee, M. H., K.-R. Kim, J.-S. Rhyee, S.-D. Park, and G. J. Snyder (2015). High Thermoelectric Figure-of-Merit in Sb<sub>2</sub>Te<sub>3</sub>/Ag<sub>2</sub>Te Bulk Composites as Pb-Free p-Type Ther-

© 2025 The Authors. Page 1093 of 1095

- moelectric Materials. Journal of Materials Chemistry C, 3; 10494–10499
- Lee, Y., S.-H. Lo, J. Androulakis, C.-I. Wu, L. Zhao, D. Y. Chung, T. P. Hogan, V. P. Dravid, and M. G. Kanatzidis (2013). High-Performance Tellurium-Free Thermoelectrics: All-Scale Hierarchical Structuring of p-Type PbSe-MSe Systems (M = Ca, Sr, Ba). *Journal of the American Chemical Society*, **135**(13); 5152–5160
- Li, J., X. Zhang, S. Lin, Z. Chen, and Y. Pei (2020). Realizing the High Thermoelectric Performance of GeTe by Sb-Doping and Se-Alloying. *Chemistry of Materials*, 32(11); 4786–4793
- Liu, Z., J. Mao, J. Liu, and Z. Ren (2022). Advances in Thermoelectrics: The Roles of Microstructures and Processing Techniques. *Materials Today Physics*, 23: 100683
- Mao, J., G. Chen, and Z. Ren (2020). Thermoelectric Cooling Materials. *Nature Materials*, **20**(4); 454–461
- Nielsen, M. D., V. Ozolins, and J. P. Heremans (2013). Lone Pair Electrons Minimize Lattice Thermal Conductivity. *Energy & Environmental Science*, **6**(2); 570–578
- Parashchuk, T., B. Wiendlocha, and et al. (2021). High Thermoelectric Performance of p-Type PbTe Enabled by the Synergy of Resonance Scattering and Lattice Softening. *ACS Applied Materials & Interfaces*, **13**(39); 46773–46784
- Pei, Y., X. Shi, A. LaLonde, H. Wang, L. Chen, and G. J. Snyder (2011). Convergence of Electronic Bands for High Performance Bulk Thermoelectrics. *Nature*, **473**(7345); 66–69
- Pei, Y., H. Wang, and G. J. Snyder (2012). Band Engineering of Thermoelectric Materials. *Advanced Materials*, **24**(46); 6125–6135
- Petsagkourakis, I., K. Tybrandt, X. Crispin, I. Ohkubo, N. Satoh, and T. Mori (2018). Thermoelectric Materials and Applications for Energy Harvesting Power Generation. *Science and Technology of Advanced Materials*, **19**(1); 836–862
- Rohendi, D., I. Amelia, N. F. Sya'baniah, D. H. Yulianti,
  N. Syarif, A. Rachmat, Fatmawati, and E. H. Majlan (2024).
  The Influence of Catalyst Loading on Electrocatalytic Activity and Hydrogen Production in PEM Water Electrolysis.
  Science and Technology Indonesia, 9(3); 556–564
- Romero, A. H., E. K. U. Gross, M. J. Verstraete, and O. Hellman (2015). Thermal Conductivity in PbTe from First Principles. *Physical Review B*, **91**(21); 214310
- Samanta, M., K. Biswas, and N. R. Desai (2018). Hole-Doping and Temperature Induced Band Inversion in Topological PbSe: Enhanced Thermoelectric Properties via Convergence of Electronic Bands. *Chemistry of Materials*, **30**(3); 989–998
- Sasidharan, N. T., V. Vaiyapuri, K. Elamurugan, N. Mani, and K. Annamalai (2025). Phonon Engineering Enabled Reduction in Thermal Conductivity of SnS/Cu<sub>2</sub>Se Composites: An Experimental and Numerical Insights. Surfaces and Interfaces, 56; 105488
- Snyder, G. J. and E. S. Toberer (2008). Complex Thermoelectric Materials. *Nature Materials*, 7(2); 105–114

- Tan, G., L. D. Zhao, and M. G. Kanatzidis (2016). Rationally Designing High-Performance Bulk Thermoelectric Materials. *Chemical Reviews*, **116**(19); 12123–12149
- Telussa, I., E. G. Fransina, E. R. M. A. P. Lilipaly, and A. M. I. Efruan (2022). Effect of Photosynthetic Pigment Composition of Tropical Marine Microalgae from Ambon Bay Navicula sp. Tad on Dye-sensitized Solar Cell Efficiency. Science and Technology Indonesia, 7(4); 486–491
- Tian, Z., J. Garg, K. Esfarjani, T. Shiga, J. Shiomi, and G. Chen (2012). Phonon Conduction in PbSe, PbTe, and PbTe<sub>1-x</sub>Se<sub>x</sub> from First-Principles Calculations. *Physical Review B*, **85**(18); 184303
- Wang, H., Z. M. Gibbs, Y. Takagiwa, and G. J. Snyder (2019). Tuning Bands of PbSe for Better Thermoelectric Efficiency. *Energy & Environmental Science*, 7(2); 804–811
- Widianingsih, S., I. Yanti, A. Kamari, and I. Fatimah (2024). Thermal Conversion of Coral Waste and its Utilization as Low-Cost Catalyst for Biodiesel Production. *Science and Technology Indonesia*, 9(4); 866–875
- Wu, H. J., L. D. Zhao, F. S. Zheng, D. Wu, Y. L. Pei, X. Tong, M. G. Kanatzidis, and J. Q. He (2014). Broad Temperature Plateau for Thermoelectric Figure of Merit ZT > 2 in Phase-Separated PbTe<sub>0.7</sub>S<sub>0.3</sub>. Nature Communications, 5(1); 5515
- Wu, L., J.-C. Zheng, J. Zhou, Q. Li, J. Yang, and Y. Zhu (2015). Nanostructures and Defects in Thermoelectric AgPb<sub>18</sub>SbTe<sub>20</sub> Single Crystal. *Journal of Applied Physics*, **105**(9); 094317
- Xiao, Y. and L. D. Zhao (2018). Charge and Phonon Transport in PbTe-Based Thermoelectric Materials. *npj Quantum Materials*, **3**(1); 29
- Yamini, S. A., T. Ikeda, A. LaLonde, Y. Pei, S. X. Dou, and G. J. Snyder (2014). Rational Design of p-Type Thermoelectric PbTe: Temperature Dependent Sodium Solubility. *Journal of Materials Chemistry A*, 1(31); 8725–8730
- Yang, L., Z.-G. Chen, G. Han, M. Hong, and J. Zou (2020). Impacts of Cu Deficiency on the Thermoelectric Properties of Cu<sub>2-X</sub>Se Nanoplates. *Nano Energy*, 69; 104394
- Yang, S., J. Si, Q. Su, and H. Wu (2022). Machine Learning in Thermoelectric Materials: A Perspective. *Energy & Environmental Materials*, 5(1); 150−171
- Zebarjadi, M., K. Esfarjani, M. S. Dresselhaus, Z. Ren, and G. Chen (2012). Perspectives on Thermoelectrics: From Fundamentals to Device Applications. *Energy & Environmental Science*, 5(1); 5147–5162
- Zhang, X. and L. D. Zhao (2015). Thermoelectric Materials: Energy Conversion Between Heat and Electricity. *Journal of Materiomics*, 1(2); 92–105
- Zhao, L. D., C. Chang, G. Tan, and M. G. Kanatzidis (2016). SnSe: A Remarkable New Thermoelectric Material. *Energy Environmental Science*, **9**(10); 3044–3060
- Zhao, L. D., V. P. Dravid, and M. G. Kanatzidis (2014a). The Panoscopic Approach to High Performance Thermoelectrics. Energy & Environmental Science, 7(1); 251–268
- Zhao, L. D., S.-H. Lo, Y. Zhang, H. Sun, G. Tan, C. Uher, C. Wolverton, V. P. Dravid, and M. G. Kanatzidis (2014b).

© 2025 The Authors. Page 1094 of 1095

Ultralow Thermal Conductivity and High Thermoelectric Figure of Merit in SnSe Crystals. *Nature*, **508**(7496); 373–377

Zhao, W., Z. Liu, P. Wei, Q. Zhang, W. Zhu, X. Su, X. Tang, J. Yang, Y. Liu, J. Shi, Y. Chao, S. Lin, and Y. Pei (2021). Flexible, Stretchable, and High-Temperature

Thermoelectric Module Based on Solution-Synthesized Tellurium Nanowires. *Nature Communications*, **12**(1); 1–10

Zhu, T., Y. Liu, C. Fu, J. P. Heremans, G. J. Snyder, and X. Zhao (2017). Compromise and Synergy in High-Efficiency Thermoelectric Materials. *Advanced Materials*, **29**(14); 1605884

© 2025 The Authors. Page 1095 of 1095